EXPLORATION OF THE PHYSICAL ORIGIN OF BLAZAR FLARES WITH A TIME-DEPENDENT ONE-ZONE MODEL

Paloma Thevenet[1], Andreas Zech[1], and Catherine Boisson[1]

[1]LUTh - Observatoire de Paris, Université PSL, Université Paris Cité, CNRS

paloma.thevenet@obspm.fr

Context

Blazars are active galactic nuclei whose relativistic jets are collimated in the line of sight of the Earth. Multi-wavelength flux variability is a well-known signature of their emission. **Rapid flares**, with variability of the order of a few days and below, are frequently observed in high-energy bands. While many interpretations exist for individual flare events, based on radiative models with varying degrees of complexity, a general picture of their physical origin is still lacking. Given the observed short variability time scales, a description based on a single compact emission region seems appropriate, if one focuses on rapid flares as isolated events.

We have explored the parameter space of a **one-zone synchrotron self-Compton model** (Maraschi et al. 1992 (*1*), Bloom & Marscher 1996 (*2*)) for different scenarios leading to flares, based on *particle injection*, *diffusive shock acceleration* and *stochastic acceleration* on turbulences (Matthews et al. 2020 (*3*)), taking into account *adiabatic expansion*. We used the time-dependent EMBLEM code (Dmytriiev 2021 (*4*)) to solve the kinetic equation describing the evolution of the electron distribution, simulate broad-band spectral distributions and multi-wavelength light curves and identify observable signatures to distinguish between these generic scenarios.

Model and EMBLEM code

The evolution of the electron distribution $N_e(\gamma, t)$ within the blob is governed by the Fokker-Planck equation (Kardashev 1962 (*5*), Tramacere et al. 2011 (*6*), Tramacere et al. 2021 (*7*)):

Cooling terms — Acceleration terms

$$\frac{\partial N_e(\gamma,t)}{\partial t} = \frac{\partial}{\partial \gamma}\left[\left(b_c(\gamma,t)\gamma^2 + \frac{1}{t_{ad}}\gamma - a(t)\gamma - \frac{2}{\gamma}D_{F_{II}}(\gamma,t)\right)N_e(\gamma,t)\right] + \frac{\partial}{\partial \gamma}\left(D_{F_{II}}(\gamma,t)\frac{\partial N_e(\gamma,t)}{\partial \gamma}\right) - N_e(\gamma,t)\left(\frac{1}{t_{esc}} + \frac{3}{t_{ad}}\right) + Q_{inj}(\gamma,t)$$

Injection term (power law)

Cooling

- Synchrotron and Inverse Compton: $b_c(\gamma, t)$
- Adiabatic expansion: $t_{ad}(t) = \frac{R(t)}{\beta_{exp} c}$
- Escape: $t_{esc}^{(turb)} = \left(\frac{R_t}{c}\right)^2 \left(\frac{\delta B}{B}\right)^2 \frac{c}{\lambda_{max}} \left(\frac{r_L}{\lambda_{max}}\right)^{q-2}$

Acceleration

- Fermi I: $a = 1/t_{shock}$
- Fermi II: $D_{F_{II}}(\gamma, t) = \frac{p^2}{t_{F_{II}}}$

$$t_{F_{II}} = \frac{1}{\beta_A^2}\left(\frac{\delta B}{B}\right)^{-2} \frac{\lambda_{max}}{c}\left(\frac{r_L}{\lambda_{max}}\right)^{2-q}$$

We denote the electron momentum p, Larmor radius r_L, (variable) Aflvén speed β_A, turbulence level $\delta B/B$, longest wavelength in the Alfvén spectrum λ_{max} and slope of the turbulent spectrum q.
Blob parameters: comoving radius R, magnetic field B, Doppler factor δ, redshift z, Lorentz factor Γ, power-law electron distribution Q_{inj}, expansion speed β_{exp}.
Evolving timescales: expansion timescale t_{ad}, turbulent escape timescale $t_{esc}^{(turb)}$, stochastic acceleration timescale $t_{F_{II}}$, synchrotron ans synchrotron self-Compton (SSC) cooling rate b_c (no external photon fields).
Fixed timescales: escape timescale t_{esc} (for no turbulence), diffusive shock acceleration timescale t_{shock}.

The EMBLEM code solves the kinetic equation using a fully implicit difference scheme by Chang & Cooper 1970 (*8*), as described by Dmytriiev 2020 (*4*).

Flare scenarios

- **Particle injection**: flaring corresponds to an **additional particle injection** in the blob for a duration $t_{dur} = 3$ observer days ≈ 8 R/c, with fixed escape timescale $t_{esc} = 1$ R/c. There is no acceleration, no blob expansion.
- **Injection and adiabatic expansion**: same flaring scenario as above including **adiabatic expansion** for an intrinsic opening angle $\alpha = \rho/\Gamma \approx 0.44°$ with $\rho = 0.26$ rad (Pushkarev et al. 2009 (*9*)).
- **Fermi II acceleration**: flaring corresponds to **stochastic acceleration** of blob particles for a duration $t_{dur} \approx 8$ R/c, with **time-dependent escape timescale** $t_{esc}^{(turb)}$. We consider only the 'hard-sphere' turbulence scenario for $q = 2$ and vary the turbulence level $0 < \delta B/B \leq 1$ and maximum wavelength $0 < \lambda_{max} \leq R$. There is no additional particle injection, no blob expansion.
- **Fermi I acceleration**: flaring corresponds to **diffusive shock acceleration** during $t_{dur} \approx 8$ R/c of timescale $t_{shock} = 1.3$ R/c, which dominates the stochastic acceleration of parameters $\delta B/B = 1$ and $\lambda_{max} = 1$. There is no additional particle injection, no blob expansion.

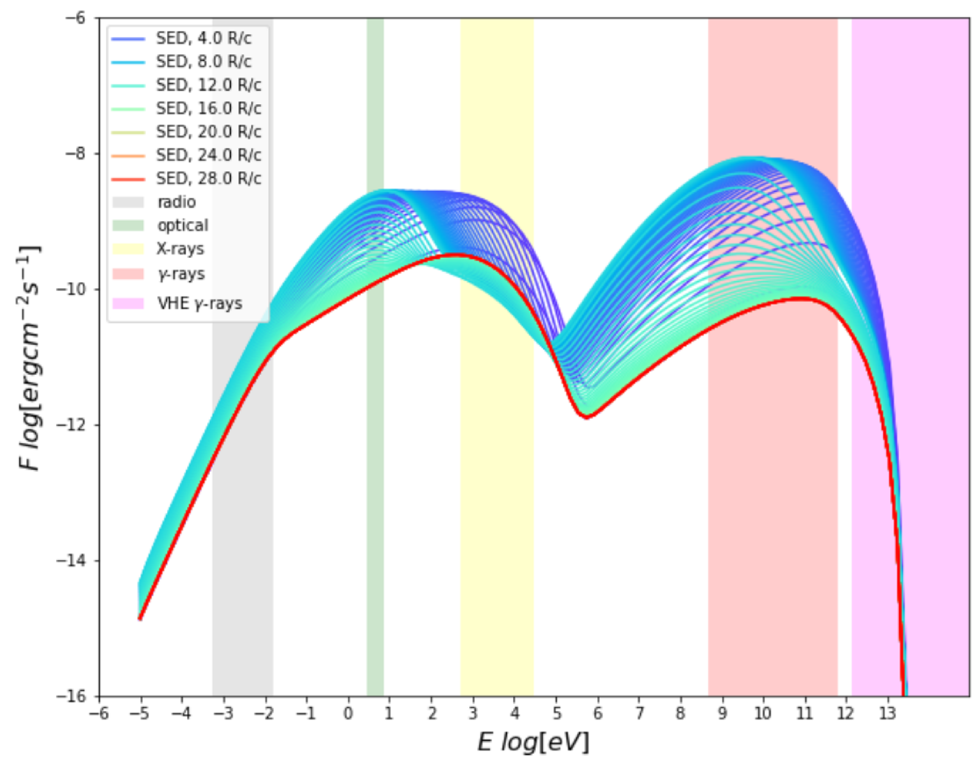

For each scenario we obtain the electron distribution evolution and the corresponding spectral energy distribution (SED). Integrating the SED in specific energy bands at each timestep, we recover the light curves (LC) for our domains of study: radio, optical, X-rays, γ-rays and VHE γ-rays.

Figure 1: SED obtained for the case of Fermi II acceleration with $\delta B/B = 1$ and $\lambda_{max} = 0.14$ R (high CD regime). The colored curves (purple - blue - green - red) represent the temporal evolution during the entire simulation. The first timestep is identical to the final one hence covered by the red curve. The vertical bands correspond to the area integrated to compute the LCs in four energy bands: radio (gray), optical (green), X-rays (yellow), γ-rays (red) and VHE γ-rays (purple).

Flare light curves

We compared LCs for four flaring scenarios given a similar X-ray maximal amplitude. However, we cannot reach such an amplitude with Fermi II acceleration for an expected Compton dominance $CD \lesssim 1$. We can reach larger X-ray amplitudes if $t_{F_{II}}$ is decreased, but the flaring enters a 'high CD regime' (Figure 3).

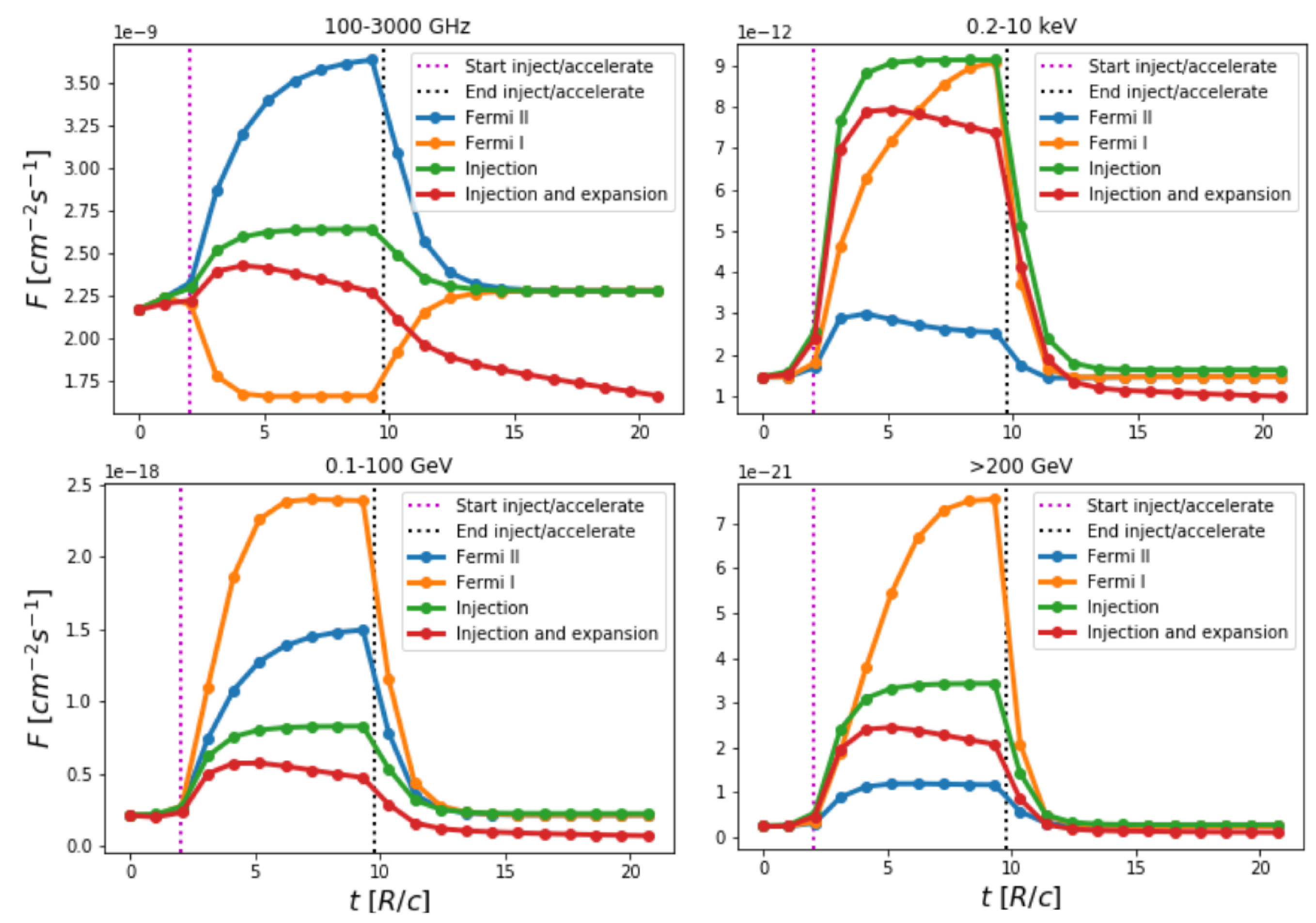

Figure 2: LCs comparison of four different flaring types. The flux evolution is given in the radio band (top left), X-ray band (top right), γ-ray band (bottom left) and VHE γ-ray band (bottom right). The Fermi II acceleration scenario is implemented with $\delta B/B = 0.5$ and $\lambda_{max} = 0.14$ R (intermediate CD regime).

Stochastic acceleration regimes

We compare the LCs for three cases of Fermi II acceleration: low ($\mathbf{t_{F_{II}} \approx 15}$ **R/c**), intermediate ($\mathbf{t_{F_{II}} \approx 6}$ **R/c**) to high ($\mathbf{t_{F_{II}} \approx 2}$ **R/c**) CD regimes, presenting different behaviours due to the piling up and cooling of high-energy electrons, as visible in the shift of the SED synchrotron and SSC bumps in Figure 1.

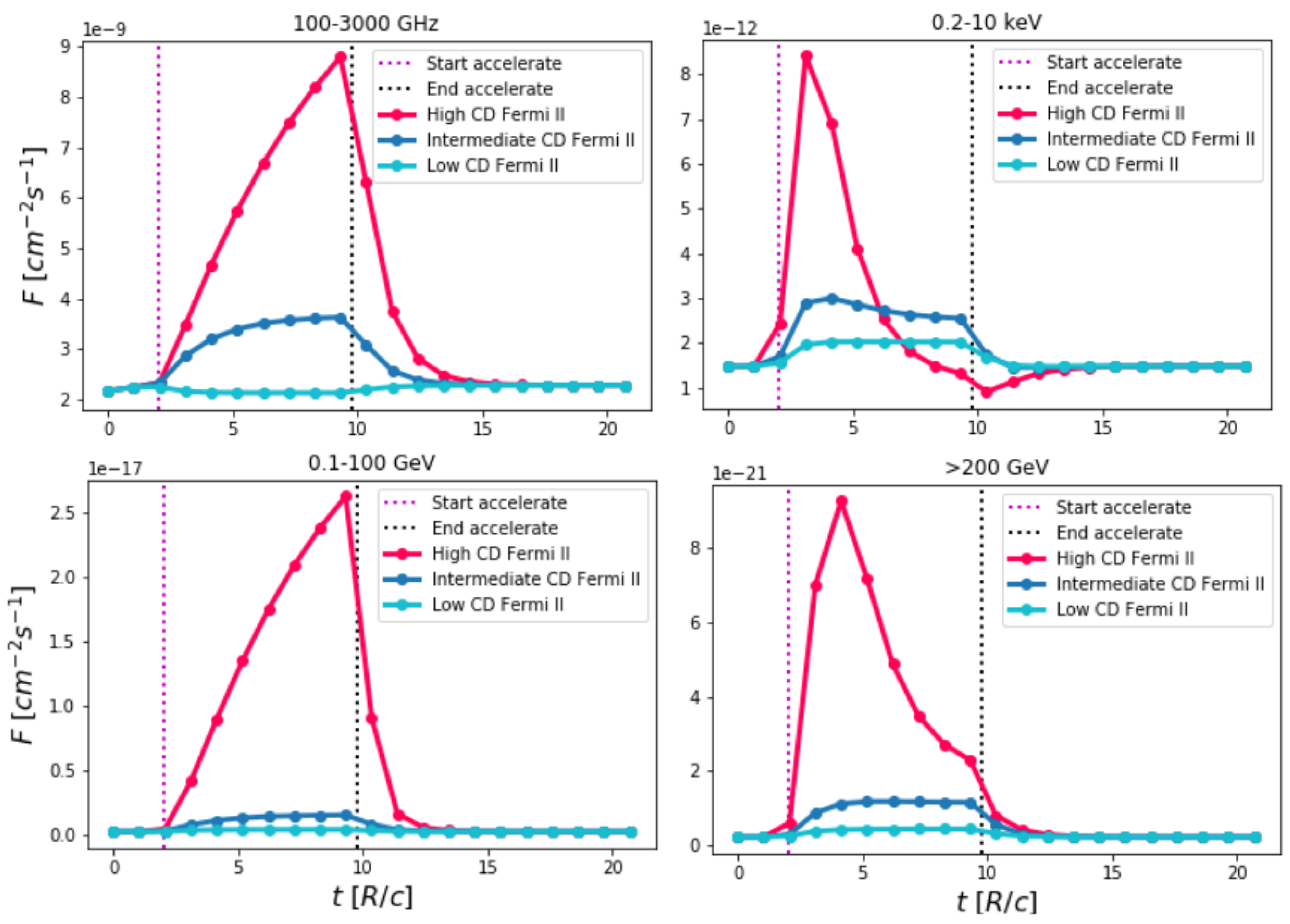

Figure 3: LCs comparison of three different Fermi II acceleration timescales. The high CD Fermi II regime is implemented with $\delta B/B = 1$ and $\lambda_{max} = 0.14$ R, the intermediate with $\delta B/B = 0.5$ and $\lambda_{max} = 0.14$ R, and the low with $\delta B/B = 1$ and $\lambda_{max} = 1$ R.

Conclusions

Exploring the parameter space, we identified LC signatures corresponding to different flaring scenarios:

- **Particle injection**: concave rise, positive half-flux asymmetry, $CD \lesssim 1$; the reaching of a plateau phase (flaring steady-state) depends on the duration t_{dur}.
- **Injection and adiabatic expansion**: decreasing quiescent emission, decreasing plateau (when reached) and negative asymmetry.
- **Low CD Fermi II acceleration**: concave rise, positive asymmetry, $CD \lesssim 1$, larger variability amplitudes (VA) of radio and γ-ray bands compared to injection.
- **High CD Fermi II acceleration**: concave/linear rise in radio, optical and γ-ray bands, convex in X-rays and VHE γ-rays, $CD > 1$, larger VA (1-2 orders of magnitude) of (V)HE γ-ray bands compared to the other domains, fast rise (negative asymmetry) and early decay in X-rays and VHE γ-rays.
  This result indicates the possibility of describing high CD flares without including external photon fields.
- **Fermi I acceleration**: CD value ($\approx$1-10) affected by the stochastic acceleration contribution, larger VA of (V)HE γ-ray bands compared to the other domains and scenarios. If $CD \lesssim 1$, plateau phase reached at different times depending on the band and shift of the SED bumps to higher frequencies during the flaring phase.

In all scenarios, the escape timescale t_{esc} and the effect of radiative cooling determine the decay time and decay shapes of the flares between energy bands.

References

1. L. Maraschi, G. Ghisellini, A. Celotti, *Astrophys. J.* **397**, L5 (1992).
2. S. D. Bloom, A. P. Marscher, *Astrophys. J.* **461**, 657 (1996).
3. J. H. Matthews, A. R. Bell, K. M. Blundell, *New Astronomy Reviews* **89**, 101543 (2020).
4. A. Dmytriiev, H. Sol, A. Zech, *Monthly Notices of the Royal Astronomical Society* **505**, 2712–2730 (2021).
5. N. S. Kardashev, *Soviet Astronomy* **6** (1962).
6. A. Tramacere, E. Massaro, A. M. Taylor, *Astrophys. J.* **739**, 66 (2011).
7. A. Tramacere, V. Sliusar, R. Walter, J. Jurysek, M. Balbo, *Astron. Astrophys.* **658**, A173 (2022).
8. J. S. Chang, G. Cooper, *J. Comput. Phys.* **6**, 1–16 (1970).
9. A. B. Pushkarev, Y. Y. Kovalev, M. L. Lister, T. Savolainen, *Astron. Astrophys.* **507**, L33 (2009).